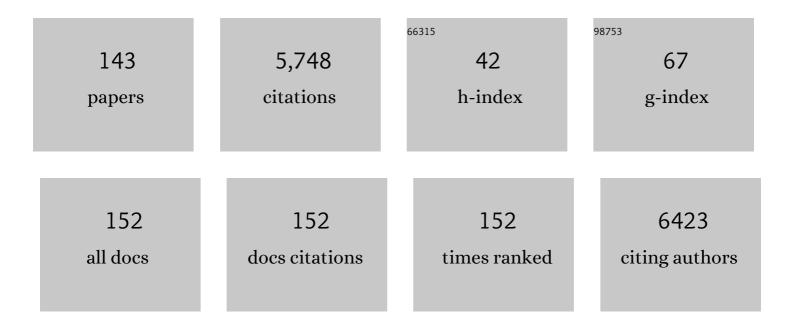
Harald E Moller

List of Publications by Year in descending order

Source: https://exaly.com/author-pdf/5104899/publications.pdf Version: 2024-02-01



HADALD F MOLLED

#	Article	IF	CITATIONS
1	MRI of the lungs using hyperpolarized noble gases. Magnetic Resonance in Medicine, 2002, 47, 1029-1051.	1.9	362
2	Spatially resolved measurements of hyperpolarized gas properties in the lung in vivo. Part I: Diffusion coefficient. Magnetic Resonance in Medicine, 1999, 42, 721-728.	1.9	170
3	Detection of emphysema in rat lungs by using magnetic resonance measurements of 3He diffusion. Proceedings of the National Academy of Sciences of the United States of America, 2000, 97, 11478-11481.	3.3	158
4	Cortical lamina-dependent blood volume changes in human brain at 7 T. NeuroImage, 2015, 107, 23-33.	2.1	152
5	Investigating Structural Brain Changes of Dehydration Using Voxel-Based Morphometry. PLoS ONE, 2012, 7, e44195.	1.1	134
6	Correcting eddy current and motion effects by affine wholeâ€brain registrations: Evaluation of threeâ€dimensional distortions and comparison with slicewise correction. Magnetic Resonance in Medicine, 2010, 64, 1047-1056.	1.9	129
7	Combined Evaluation of FDG-PET and MRI Improves Detection and Differentiation of Dementia. PLoS ONE, 2011, 6, e18111.	1.1	129
8	Iron, Myelin, and the Brain: Neuroimaging Meets Neurobiology. Trends in Neurosciences, 2019, 42, 384-401.	4.2	123
9	Sex-Dependent Influences of Obesity on Cerebral White Matter Investigated by Diffusion-Tensor Imaging. PLoS ONE, 2011, 6, e18544.	1.1	121
10	Differential effects of global and cerebellar normalization on detection and differentiation of dementia in FDG-PET studies. NeuroImage, 2010, 49, 1490-1495.	2.1	118
11	White matter abnormalities in patients with treated hyperphenylalaninaemia: Magnetic resonance relaxometry and proton spectroscopy findings. European Journal of Pediatrics, 1993, 152, 1012-1020.	1.3	109
12	Slab-selective, BOLD-corrected VASO at 7 Tesla provides measures of cerebral blood volume reactivity with high signal-to-noise ratio. Magnetic Resonance in Medicine, 2014, 72, 137-148.	1.9	107
13	Investigation of the neurovascular coupling in positive and negative BOLD responses in human brain at 7T. NeuroImage, 2014, 97, 349-362.	2.1	101
14	Myelin water mapping by spatially regularized longitudinal relaxographic imaging at high magnetic fields. Magnetic Resonance in Medicine, 2014, 71, 375-387.	1.9	97
15	Retinotopic activation in response to subjective contours in primary visual cortex. Frontiers in Human Neuroscience, 2008, 2, 1-7.	1.0	96
16	Non-BOLD contrast for laminar fMRI in humans: CBF, CBV, and CMRO2. NeuroImage, 2019, 197, 742-760.	2.1	96
17	MR microscopy of lung airways with hyperpolarized3He. Magnetic Resonance in Medicine, 1998, 39, 79-84.	1.9	95
18	Localized proton NMR spectroscopy in the striatum of patients with idiopathic parkinson's disease: a multicenter pilot study. Magnetic Resonance in Medicine, 1995, 33, 589-594.	1.9	91

#	Article	lF	CITATIONS
19	Real diffusion-weighted MRI enabling true signal averaging and increased diffusion contrast. NeuroImage, 2015, 122, 373-384.	2.1	88
20	Normal Clinical Outcome in Untreated Subjects with Mild Hyperphenylalaninemia. Pediatric Research, 2001, 49, 532-536.	1.1	83
21	Spatially resolved measurements of hyperpolarized gas properties in the lung in vivo. Part II:T?2. Magnetic Resonance in Medicine, 1999, 42, 729-737.	1.9	81
22	Individual blood-brain barrier phenylalanine transport determines clinical outcome in phenylketonuria. Annals of Neurology, 2001, 50, 463-467.	2.8	78
23	Blood—Brain Barrier Phenylalanine Transport and Individual Vulnerability in Phenylketonuria. Journal of Cerebral Blood Flow and Metabolism, 1998, 18, 1184-1191.	2.4	71
24	Quantifying the intra- and extravascular contributions to spin-echo fMRI at 3 T. Magnetic Resonance in Medicine, 2004, 52, 724-732.	1.9	68
25	Pathological glutamatergic neurotransmission in Gilles de la Tourette syndrome. Brain, 2017, 140, 218-234.	3.7	68
26	Lamina-dependent calibrated BOLD response in human primary motor cortex. NeuroImage, 2016, 141, 250-261.	2.1	66
27	Signal Dynamics in Magnetic Resonance Imaging of the Lung with Hyperpolarized Noble Gases. Journal of Magnetic Resonance, 1998, 135, 133-143.	1.2	65
28	Simultaneous Quantitative MRI Mapping of T1, T2* and Magnetic Susceptibility with Multi-Echo MP2RAGE. PLoS ONE, 2017, 12, e0169265.	1.1	65
29	Functional MR microscopy of the lung using hyperpolarized3He. Magnetic Resonance in Medicine, 1999, 41, 787-792.	1.9	62
30	Neurocognitive functioning in adults with phenylketonuria: Results of a long term study. Molecular Genetics and Metabolism, 2013, 110, S44-S48.	0.5	62
31	Orientation dependence of magnetization transfer parameters in human white matter. Neurolmage, 2015, 114, 136-146.	2.1	62
32	Physical exercise in overweight to obese individuals induces metabolic- and neurotrophic-related structural brain plasticity. Frontiers in Human Neuroscience, 2015, 9, 372.	1.0	61
33	Investigating brain response to music: A comparison of different fMRI acquisition schemes. NeuroImage, 2011, 54, 337-343.	2.1	59
34	Magnetic resonance spectroscopy in patients with MELAS. Journal of the Neurological Sciences, 2005, 229-230, 131-139.	0.3	58
35	Carbon-wire loop based artifact correction outperforms post-processing EEG/fMRI corrections—A validation of a real-time simultaneous EEG/fMRI correction method. NeuroImage, 2016, 125, 880-894.	2.1	58
36	Functional perfusion imaging using continuous arterial spin labeling with separate labeling and imaging coils at 3 T. Magnetic Resonance in Medicine, 2003, 49, 791-795.	1.9	56

#	Article	IF	CITATIONS
37	Pulmonary Perfusion and Xenon Gas Exchange in Rats: MR Imaging with Intravenous Injection of Hyperpolarized ¹²⁹ Xe. Radiology, 2009, 252, 386-393.	3.6	55
38	Metabolic characterization of AIDS dementia complex by spectroscopic imaging. Journal of Magnetic Resonance Imaging, 1999, 9, 10-18.	1.9	54
39	Magnetic resonance angiography with hyperpolarized129Xe dissolved in a lipid emulsion. Magnetic Resonance in Medicine, 1999, 41, 1058-1064.	1.9	54
40	Commentary: Cluster failure: Why fMRI inferences for spatial extent have inflated false-positive rates. Frontiers in Human Neuroscience, 2017, 11, 345.	1.0	53
41	Measurements of hyperpolarized gas properties in the lung. part III:3HeT1. Magnetic Resonance in Medicine, 2001, 45, 421-430.	1.9	50
42	Kinetics of phenylalanine transport at the human blood–brain barrier investigated in vivo. Brain Research, 1997, 778, 329-337.	1.1	49
43	Resting-state functional magnetic resonance imaging of the subthalamic microlesion and stimulation effects in Parkinson's disease: Indications of a principal role of the brainstem. NeuroImage: Clinical, 2015, 9, 264-274.	1.4	46
44	Brain Damage With Heart Failure. Circulation Research, 2020, 126, 750-764.	2.0	45
45	In-Vivo NMR Spectroscopy in Patients with Phenylketonuria: Changes of Cerebral Phenylalanine Levels Under Dietary Treatment. Neuropediatrics, 1995, 26, 199-202.	0.3	43
46	Brain connectivity changes when comparing effects of subthalamic deep brain stimulation with levodopa treatment in Parkinson's disease. NeuroImage: Clinical, 2018, 19, 1025-1035.	1.4	43
47	Multicenter Study of Subjective Acceptance During Magnetic Resonance Imaging at 7 and 9.4 T. Investigative Radiology, 2014, 49, 249-259.	3.5	42
48	Investigating the dynamics of the brain response to music: A central role of the ventral striatum/nucleus accumbens. NeuroImage, 2015, 116, 68-79.	2.1	41
49	Individual blood-brain barrier phenylalanine transport in siblings with classical phenylketonuria. Journal of Inherited Metabolic Disease, 2002, 25, 431-436.	1.7	40
50	Impact of image acquisition on voxel-based-morphometry investigations of age-related structural brain changes. NeuroImage, 2014, 87, 170-182.	2.1	40
51	In vivo NMR spectroscopy in patients with phenylketonuria: Clinical significance of interindividual differences in brain phenylalanine concentrations. Journal of Inherited Metabolic Disease, 1998, 21, 81-82.	1.7	39
52	Sensitivity and resolution in 3D NMR microscopy of the lung with hyperpolarized noble gases. Magnetic Resonance in Medicine, 1999, 41, 800-808.	1.9	39
53	Whole-brain mapping of venous vessel size in humans using the hypercapnia-induced BOLD effect. NeuroImage, 2010, 51, 765-774.	2.1	39
54	Development and Evaluation of an Algorithm for the Computer-Assisted Segmentation of the Human Hypothalamus on 7-Tesla Magnetic Resonance Images. PLoS ONE, 2013, 8, e66394.	1.1	37

#	Article	IF	CITATIONS
55	In vivo magnetic resonance vascular imaging using laser-polarized 3He microbubbles. Proceedings of the United States of America, 1998, 95, 10832-10835.	3.3	35
56	Baseline oxygenation in the brain: Correlation between respiratory-calibration and susceptibility methods. NeuroImage, 2016, 125, 920-931.	2.1	35
57	The effect of local perturbation fields on human DTI: Characterisation, measurement and correction. NeuroImage, 2012, 60, 562-570.	2.1	33
58	Brain imaging and proton magnetic resonance spectroscopy in patients with phenylketonuria. Pediatrics, 2003, 112, 1580-3.	1.0	33
59	A unified 3D map of microscopic architecture and MRI of the human brain. Science Advances, 2022, 8, eabj7892.	4.7	33
60	Mixing oxygen with hyperpolarized3He for small-animal lung studies. NMR in Biomedicine, 2000, 13, 202-206.	1.6	32
61	In vivo proton magnetic resonance spectroscopy in phenylketonuria. European Journal of Pediatrics, 2000, 159, S121-S125.	1.3	32
62	Continuously Infusing Hyperpolarized 129Xe into Flowing Aqueous Solutions Using Hydrophobic Gas Exchange Membranes. Journal of Physical Chemistry B, 2009, 113, 12489-12499.	1.2	31
63	Therapy of complex I deficiency: Peripheral neuropathy during dichloroacetate therapy. European Journal of Pediatrics, 1995, 154, 928-932.	1.3	30
64	Dynamic hysteresis between gradient echo and spin echo attenuations in dynamic susceptibility contrast imaging. Magnetic Resonance in Medicine, 2013, 69, 981-991.	1.9	30
65	Efficiency of flow-driven adiabatic spin inversion under realistic experimental conditions: A computer simulation. Magnetic Resonance in Medicine, 2004, 51, 1187-1193.	1.9	29
66	Continuous arterial spin labeling at the human common carotid artery: the influence of transit times. NMR in Biomedicine, 2005, 18, 19-23.	1.6	25
67	Is there a change in water proton density associated with functional magnetic resonance imaging?. Magnetic Resonance in Medicine, 2005, 53, 470-473.	1.9	25
68	Increasing specificity in functional magnetic resonance imaging by estimation of vessel size based on changes in blood oxygenation. NeuroImage, 2008, 40, 228-236.	2.1	25
69	Cortical laminar restingâ€state signal fluctuations scale with the hypercapnic blood oxygenation levelâ€dependent response. Human Brain Mapping, 2020, 41, 2014-2027.	1.9	25
70	Increased sensitivity and signal-to-noise ratio in diffusion-weighted MRI using multi-echo acquisitions. Neurolmage, 2020, 221, 117172.	2.1	24
71	BOLD background gradient contributions in diffusionâ€weighted fMRI—comparison of spinâ€echo and twiceâ€refocused spinâ€echo sequences. NMR in Biomedicine, 2010, 23, 610-618.	1.6	23
72	Mapping of arterial transit time by intravascular signal selection. NMR in Biomedicine, 2014, 27, 594-609.	1.6	23

#	Article	IF	CITATIONS
73	Effect of 3T MRI on the function of shunt valves—Evaluation of Paedi GAV, Dual Switch and proGAV. European Journal of Radiology, 2005, 56, 56-59.	1.2	22
74	Functional cerebral blood volume mapping with simultaneous multi-slice acquisition. NeuroImage, 2016, 125, 1159-1168.	2.1	22
75	Application of NMR spectroscopy to monitoring MELAS treatment: A case report. Muscle and Nerve, 2002, 25, 593-600.	1.0	21
76	A Modified EPI sequence for highâ€resolution imaging at ultraâ€short echo time. Magnetic Resonance in Medicine, 2011, 65, 165-175.	1.9	21
77	TS-EUROTRAIN: A European-Wide Investigation and Training Network on the Etiology and Pathophysiology of Gilles de la Tourette Syndrome. Frontiers in Neuroscience, 2016, 10, 384.	1.4	21
78	7 Tesla MRI Followed by Histological 3D Reconstructions in Whole-Brain Specimens. Frontiers in Neuroanatomy, 2020, 14, 536838.	0.9	21
79	Hyperpolarized3He NMR Lineshape Measurements in the Live Guinea Pig Lung. Magnetic Resonance in Medicine, 1998, 40, 61-65.	1.9	20
80	A comparison of signal instability in 2D and 3D EPI resting-state fMRI. NMR in Biomedicine, 2005, 18, 534-542.	1.6	20
81	Functional magnetic resonance imaging with intermolecular double-quantum coherences at 3 T. Magnetic Resonance in Medicine, 2005, 53, 1402-1408.	1.9	20
82	Towards quantification of blood-flow changes during cognitive task activation using perfusion-based fMRI. NeuroImage, 2005, 27, 919-926.	2.1	20
83	Functional contrast based on intermolecular doubleâ€quantum coherences: Influence of the correlation distance. Magnetic Resonance in Medicine, 2007, 58, 696-704.	1.9	20
84	In Vivo MR Imaging of Pulmonary Perfusion and Gas Exchange in Rats via Continuous Extracorporeal Infusion of Hyperpolarized 129Xe. PLoS ONE, 2012, 7, e31306.	1.1	20
85	Diffusion imaging-based subdivision of the human hypothalamus: a magnetic resonance study with clinical implications. European Archives of Psychiatry and Clinical Neuroscience, 2013, 263, 497-508.	1.8	20
86	Dynamic metabolic changes in human visual cortex in regions with positive and negative blood oxygenation level-dependent response. Journal of Cerebral Blood Flow and Metabolism, 2019, 39, 2295-2307.	2.4	20
87	In vivo study of brain metabolism in galactosemia by1H and31P magnetic resonance spectroscopy. European Journal of Pediatrics, 1995, 154, S8-S13.	1.3	19
88	Is there a hazard to health by mercury exposure from amalgam due to MRI?. Journal of Magnetic Resonance Imaging, 1996, 6, 258-260.	1.9	19
89	Tackling frontal lobe–related functions in PKU through functional brain imaging: a Stroop task in adult patients. Journal of Inherited Metabolic Disease, 2011, 34, 711-721.	1.7	18
90	Differential effects of deep brain stimulation and levodopa on brain activity in Parkinson's disease. Brain Communications, 2020, 2, fcaa005.	1.5	18

#	Article	IF	CITATIONS
91	In Vivo31P NMR Spectroscopy of Human Musculoskeletal Tumors as a Measure of Response to Chemotherapy. , 1996, 9, 347-358.		17
92	Relaxation of hyperpolarized 129Xe in a deflating polymer bag. Journal of Magnetic Resonance, 2011, 212, 109-115.	1.2	17
93	Temperature dependence of water diffusion pools in brain white matter. NeuroImage, 2016, 127, 135-143.	2.1	17
94	Cardiac cycle-induced EPI time series fluctuations in the brain: Their temporal shifts, inflow effects and T2â^— fluctuations. NeuroImage, 2017, 162, 93-105.	2.1	17
95	Magnetic resonance imaging of hyperpolarized 129Xe produced by spin exchange with diode-laser pumped Cs. Applied Physics Letters, 1998, 73, 2666-2668.	1.5	16
96	Matrix-algebra-based calculations of the time evolution of the binary spin-bath model for magnetization transfer. Journal of Magnetic Resonance, 2013, 230, 88-97.	1.2	16
97	Modulatory Effects of Levodopa on Cerebellar Connectivity in Parkinson's Disease. Cerebellum, 2019, 18, 212-224.	1.4	16
98	Dual regression physiological modeling of resting-state EPI power spectra: Effects of healthy aging. NeuroImage, 2019, 187, 68-76.	2.1	16
99	MR flow quantification using race: Clinical application to the carotid arteries. Journal of Magnetic Resonance Imaging, 1996, 6, 503-512.	1.9	15
100	Creatine loading and resting skeletal muscle phosphocreatine flux: a saturation-transfer NMR study. Magnetic Resonance Materials in Physics, Biology, and Medicine, 2001, 13, 118-126.	1.1	15
101	A semi-automated algorithm for hypothalamus volumetry in 3 Tesla magnetic resonance images. Psychiatry Research - Neuroimaging, 2018, 277, 45-51.	0.9	15
102	No evidence for individual blood-brain barrier phenylalanine transport to influence clinical outcome in typical phenylketonuria patients. Annals of Neurology, 2002, 52, 382-383.	2.8	14
103	Pathogenesis of different clinical outcomes in spite of identical genotypes and comparable blood phenylalanine concentrations in phenylketonurics. Journal of Inherited Metabolic Disease, 1998, 21, 181-182.	1.7	13
104	Shielded dualâ€loop resonator for arterial spin labeling at the neck. Journal of Magnetic Resonance Imaging, 2009, 29, 1414-1424.	1.9	11
105	Serum BDNF correlates with connectivity in the (pre)motor hub inÂthe aging human brain—a resting-state fMRI pilot study. Neurobiology of Aging, 2016, 38, 181-187.	1.5	11
106	PyRates—A Python framework for rate-based neural simulations. PLoS ONE, 2019, 14, e0225900.	1.1	11
107	Gradient-induced longitudinal relaxation of hyperpolarized noble gases in the fringe fields of superconducting magnets used for magnetic resonance. Journal of Magnetic Resonance, 2011, 208, 284-290.	1.2	10
108	Centerâ€out echoâ€planar spectroscopic imaging with correction of gradientâ€echo phase and time shifts. Magnetic Resonance in Medicine, 2013, 70, 16-24.	1.9	10

#	Article	IF	CITATIONS
109	Motor Matters: Tackling Heterogeneity of Parkinson's Disease in Functional MRI Studies. PLoS ONE, 2013, 8, e56133.	1.1	10
110	Disease-Specific Regions Outperform Whole-Brain Approaches in Identifying Progressive Supranuclear Palsy: A Multicentric MRI Study. Frontiers in Neuroscience, 2017, 11, 100.	1.4	10
111	Semiâ€automated generation of individual computational models of the human head and torso from MR images. Magnetic Resonance in Medicine, 2019, 81, 2090-2105.	1.9	10
112	Carboxymethyldextran-A2-Gd-DOTA enhancement patterns in the abdomen and pelvis in an animal model. European Radiology, 2001, 11, 1276-1284.	2.3	9
113	A microstrip helmet coil for human brain imaging at high magnetic fields. Concepts in Magnetic Resonance Part B, 2008, 33B, 94-108.	0.3	9
114	Accounting for Movement Increases Sensitivity in Detecting Brain Activity in Parkinson's Disease. PLoS ONE, 2012, 7, e36271.	1.1	9
115	Obesity Associated Cerebral Gray and White Matter Alterations Are Interrelated in the Female Brain. PLoS ONE, 2014, 9, e114206.	1.1	9
116	Macromolecular background signal and <scp>nonâ€Gaussian</scp> metabolite diffusion determined in human brain using ultraâ€high diffusion weighting. Magnetic Resonance in Medicine, 2022, 88, 1962-1977.	1.9	9
117	Investigation of higherâ€order cognitive functions during exposure to a high static magnetic field. Journal of Magnetic Resonance Imaging, 2012, 36, 835-840.	1.9	8
118	Characterization of pseudoâ€continuous arterial spin labeling: Simulations and experimental validation. Magnetic Resonance in Medicine, 2018, 79, 1638-1649.	1.9	8
119	Kinetics of Metabolism in Human Kidney Transplants Measured by Dynamic 31P NMR Spectroscopy. Zeitschrift Fur Naturforschung - Section C Journal of Biosciences, 1995, 50, 439-450.	0.6	7
120	Combined PET/MRI. Neurology, 2016, 86, 1926-1927.	1.5	7
121	Tissue pH in human kidney transplants during hypothermic ischemia. Magnetic Resonance Imaging, 2000, 18, 743-751.	1.0	6
122	Reengineered helmet coil for human brain studies at 3 Tesla. Concepts in Magnetic Resonance Part B, 2005, 27B, 64-74.	0.3	6
123	Transient signal changes in diffusion-weighted stimulated echoes during neuronal stimulation at 3T. Journal of Magnetic Resonance Imaging, 2007, 25, 947-956.	1.9	6
124	Influence of the extracellular matrix on water mobility in subcortical gray matter. Magnetic Resonance in Medicine, 2019, 81, 1265-1279.	1.9	6
125	Quantifying venous flow dynamics by flow-dephased and flow-rephased functional magnetic resonance imaging. Magnetic Resonance Materials in Physics, Biology, and Medicine, 2005, 18, 272-275.	1.1	5
126	A new approach to <i>Z</i> â€spectrum acquisition: prospective baseline enhancement (PROBE) for CEST/Nuclear Overhauser Effect. Magnetic Resonance in Medicine, 2019, 81, 2315-2329.	1.9	5

#	Article	IF	CITATIONS
127	Modeling radio-frequency energy-induced heating due to the presence of transcranial electric stimulation setup at 3T. Magnetic Resonance Materials in Physics, Biology, and Medicine, 2020, 33, 793-807.	1.1	5
128	Assessment of Collateral Supply by Two-Coil Continuous Arterial Spin Labeling after Coil Occlusion of the Internal Carotid Artery. American Journal of Neuroradiology, 2007, 28, 1304-1305.	1.2	4
129	Hypercapniaâ€induced effects on image contrast based on intermolecular doubleâ€quantum coherences. Magnetic Resonance in Medicine, 2008, 60, 1306-1312.	1.9	4
130	"Eyes Open – Eyes Closed―EEG/fMRI data set including dedicated "Carbon Wire Loop―motion detect channels. Data in Brief, 2016, 7, 990-994.	ion 0.5	4
131	Three-dimensional echo-planar cine imaging of cerebral blood supply using arterial spin labeling. Magnetic Resonance Materials in Physics, Biology, and Medicine, 2016, 29, 799-810.	1.1	4
132	Serial proton spectroscopy in a case of adult-onset subacute sclerosing panencephalitis. Psychiatry Research - Neuroimaging, 2005, 139, 269-273.	0.9	3
133	Modulation of premotor cortex response to sequence motor learning during escitalopram intake. Journal of Cerebral Blood Flow and Metabolism, 2021, 41, 1449-1462.	2.4	3
134	Deconvolutionâ€based distortion correction of EPI using analytic singleâ€voxel pointâ€spread functions. Magnetic Resonance in Medicine, 2021, 85, 2445-2461.	1.9	3
135	Magnetization‒transfer31P NMR of biochemical exchangein vivo: Application to creatine kinase kinetics. Spectroscopy, 2002, 16, 207-216.	0.8	2
136	Localized proton NMR spectroscopy in the striatum of patients with idiopathic spasmodic torticollis. Magnetic Resonance in Medicine, 1998, 39, 309-312.	1.9	1
137	Selfâ€assessed and objective blood phenylalanine levels in patients with early treated phenylketonuria. Acta Paediatrica, International Journal of Paediatrics, 2010, 99, 944-945.	0.7	1
138	Extracting Regional Oxygen Tension from Multibreath Wash-in3He MR Imaging. Radiology, 2017, 285, 1056-1057.	3.6	1
139	Modeling Electromagnetic Exposure in Humans Inside a Whole-Body Birdcage Coil Excited by a Two-Channel Parallel Transmitter Operated at 123 MHz. IEEE Journal of Electromagnetics, RF and Microwaves in Medicine and Biology, 2020, 4, 247-253.	2.3	1
140	Decreased thalamo-cortico connectivity during an implicit sequence motor learning task and 7Âdays escitalopram intake. Scientific Reports, 2021, 11, 15060.	1.6	1
141	In Vivo 31P NMR Spectroscopy of Human Musculoskeletal Tumors as a Measure of Response to Chemotherapy. NMR in Biomedicine, 1996, 9, 347-358.	1.6	1
142	Effects of the geometry and size of the cerebrospinal fluid on MRI transmit and safety efficiencies at 300 MHz. , 2016, 2016, 2909-2912.		0
143	Measuring Arterial Pulsatility With Dynamic Inflow Magnitude Contrast. Frontiers in Neuroscience, 2021, 15, 795749.	1.4	0